Published in final edited form as:

Endocr Relat Cancer. 2020 April ; 27(4): 261–274. doi:10.1530/ERC-19-0431.

Neutrophil Elastase from Myeloid Cells Promotes TSC2-null Tumor Growth

Manisha Taya[1], **Maria de la Luz Garcia-Hernandez**[2], **Javier Rangel-Moreno**[2], **Briaunna Minor**[1], **Erin Gibbons**[1], **Stephen R Hammes**[1]

[1]Division of Endocrinology, Diabetes, and Metabolism, Department of Medicine, University of Rochester Medical Center, Rochester, NY

[2]Division of Allergy/Immunology and Rheumatology, Department of Medicine, University of Rochester Medical Center, Rochester, NY.

Abstract

Chronic inflammation promotes progression of many cancers, with circulating myeloid-derived suppressor cell (MDSC) levels correlating with poor prognosis. Here we examine effects of MDSCs on lymphangioleiomyomatosis (LAM), a rare disease occurring almost exclusively in women whereby estrogen-sensitive metastatic TSC2-null tumors grow throughout the lungs, markedly reducing pulmonary function. The LAM cell origin remains unknown; however, previous work demonstrated that *Tsc2* inactivation in the mouse uterus induced estrogen-dependent myometrial tumors with nearly all features of LAM. Half of these animals developed metastatic myometrial tumors in the lungs, suggesting that LAM cells might originate from the myometrium, possibly explaining its overwhelming female prevalence and estrogen-sensitivity. Here we report that MDSC levels, and in particular granulocytic myeloid cell levels, are elevated in the periphery and in tumors of uterine-specific *Tsc2*-null mice. Importantly, MDSC depletion or inhibition of their recruitment impairs myometrial tumor growth. RNA and protein analysis of *Tsc2*-null myometrial tumors and xenografts demonstrate high expression and activity of the serine protease neutrophil elastase (NE), with selective qPCR studies indicating a stromal origin of the NE. Notably, treatment with sivelestat, a known NE inhibitor already approved for human use in some countries, reduces tumor growth similar to MDSC depletion. Furthermore, NE promotes *Tsc2*-null tumor cell growth, migration, and invasion *in-vitro*. Finally, NE-expressing myeloid cells are present throughout the lungs of LAM patients but not controls. These data suggest that NE derived from granulocytic myeloid cells, might directly promote LAM tumor cell progression and could be a novel therapeutic target for LAM.

Corresponding author: Stephen R Hammes, University of Rochester Medical Center, 601 Elmwood Ave, Box 693, Rochester, NY 14642; 585-276-4994; stephen_hammes@urmc.rochester.edu.

Author contributions

Conception and design of research studies: M. Taya, S.R. Hammes

Conducting experiments, acquisition of data: M. Taya, M.L. Garcia-Hernandez, J. Rangel-Moreno, B. Minor, E. Gibbons

Analysis and interpretation of data: M. Taya, M.L. Garcia-Hernandez, J. Rangel-Moreno, B. Minor, E. Gibbons, S.R. Hammes

Writing/reviewing the manuscript: M. Taya, S.R. Hammes

Study supervision: S.R. Hammes

Conflicts

There are no known conflicts of interest with any of the authors.

Keywords

Neutrophil Elastase; myeloid-derived suppressor cell; lymphangioleiomomatosis; estrogen

Introduction

Lymphangioleiomyomatosis (LAM) is a rare, devastating pulmonary lung disease almost exclusively affecting women in their reproductive years whereby estrogen-sensitive metastatic smooth-muscle cell-like adenomas grow within the lungs, insidiously driving loss of pulmonary function (Kelly and Moss 2001). LAM affects approximately 300,000 individuals worldwide (Ferrans, et al. 2000; Krymskaya 2008; McCormack 2006) and is often initially misdiagnosed or diagnosed at a late stage, which can lead to death due to respiratory failure. LAM cells contain mutations in tumor suppressor tuberous sclerosis 1 or 2 (*TSC1* or *TSC2*) genes, resulting in heightened mammalian target of rapamycin complex1 (mTORC1) activity and cell proliferation (Carsillo, et al. 2000; Smolarek, et al. 1998). mTORC1 inhibitors, the only FDA approved treatment for LAM, slow LAM progression but do not eliminate LAM tumors (Ando, et al. 2013; McCormack, et al. 2011; Taveira-Dasilva, et al. 2011). In addition, these drugs have immunosuppressive actions and other significant side effects, making development of alternative treatments critical. Notably, the last treatment for LAM patients experiencing loss in pulmonary function is lung transplantation; however, probability of disease recurrence in the transplanted lungs is high (Bittmann, et al. 2003; Karbowniczek, et al. 2003), suggesting a metastatic nature of the tumors.

Given the marked female sexual dimorphism, the estrogen-sensitivity, the smooth muscle nature of LAM tumor cells, and the metastatic nature of LAM, we previously hypothesized that lung LAM cells may be metastatic from the uterine myometrium. In fact, 90% of LAM patients undergoing hysterectomies had uterine LAM lesions (Hayashi, et al. 2011). We therefore inactivated the *Tsc2* gene in the mouse uterus and demonstrated that all female mice developed myometrial tumors with nearly all features of LAM, including heightened mTORC1 activity, estrogen and progesterone receptor expression, and over-expression of melanocytic markers pathognomonic of LAM tumor cells. By 34-weeks, approximately 50% of animals developed metastatic myometrial tumors in the lung, suggesting that lung LAM cells might originate from the uterine myometrium (Prizant, et al. 2013). Estrogen ablation caused nearly complete regression of *Tsc2*-null myometrial tumors, as well as loss of mTORC1 activity, indicating that, even without Tsc2, estradiol is required to maintain mTORC1 activity and tumor growth in this mouse model (Prizant, et al. 2016). Through RNAseq analysis of *Tsc2*-null uterine tumors, we identified the protease neutrophil elastase (NE) as being highly expressed in *Tsc2*-null uterine tumors. Immunohistochemistry confirmed heterogeneous NE protein expression in *Tsc2*-null uterine tumors, and using an *in-vivo* NE-sensitive optical probe, we demonstrated NE enzyme activity in tumors (Prizant, et al. 2016).

NE is primarily expressed in and secreted by neutrophils, and plays an important role in innate host defense during infection and disease. In addition, NE is a key player in critical inflammatory responses that lead to pro-tumorigenic phenotypes such as proliferation,

epithelial-mesenchymal transition (EMT), migration, invasion, and metastasis in numerous cancers including lung, prostate, colorectal, and breast (El Rayes, et al. 2015; Grosse-Steffen, et al. 2012; Houghton, et al. 2010; Lerman, et al. 2017; Wada, et al. 2007; Yamashita, et al. 1997). Elevated NE activity is seen in sera from colon and lung cancer patients compared to healthy individuals, with increased activity correlating with disease progression (Ho, et al. 2014; Vaguliene, et al. 2013). Finally, in mouse cancer models, NE knockout reduces tumor growth and metastasis, supporting an important role for NE in cancer progression (Gong, et al. 2013; Ho, et al. 2014; Houghton, et al. 2010).

Data from our lab and others suggest that NE is also present in granulocytic myeloid-derived suppressor cells (MDSCs) (Lerman, et al. 2017; Youn, et al. 2012). MDSCs are a heterogeneous population of immature myeloid cells that have not terminally differentiated into mature myeloid cells such as granulocytes (neutrophils), macrophages, or dendritic cells (Marvel and Gabrilovich 2015). MDSCs are not in the circulation under normal physiological conditions, but increased accumulation of the MDSCs is implicated in pathological conditions including chronic inflammation, autoimmune diseases, infection, trauma, and cancers (Dumitru, et al. 2013; Zhou, et al. 2018). MDSC populations are expanded in the blood and stroma of cancers such as breast, lung, melanoma, and prostate, and tumor cells may secrete cytokines and chemokines that stimulate MDSC production in bone marrow and their eventual infiltration into tumor beds (Alfaro, et al. 2016; Lerman and Hammes 2018; Marvel and Gabrilovich 2015; Wang, et al. 2016). MDSCs express CD11b and Gr1 (Ly6G/Ly6C) cell surface markers that characterize MDSCs into two subsets, polymorphonuclear, or PMN-MDSCs ($CD11b^{+}Ly6G^{+}Ly6C^{low}$)(also called granulocytic, or G-MDSCs), and monocytic MDSCs or M-MDSCs ($CD11b^{+}Ly6G^{-}Ly6C^{high}$). M-MDSCs primarily exhibit immune-suppressive functions that facilitate tumor progression, whereas G-MDSCs represent 80% of all MDSCs and may directly promote tumor growth (Dumitru, et al. 2012; Marvel and Gabrilovich 2015) in addition to being immunosuppressive. Multiple studies report reduced tumor progression following G-MDSC depletion (Gabrilovich, et al. 2012; Galdiero, et al. 2018; Lerman, et al. 2017).

In the present study we defined the role of MDSCs in *Tsc2*-null tumor progression, hypothesizing that NE from infiltrating granulocytic MDSCs/neutrophils may promote LAM tumor progression. We confirmed that NE is expressed in surrounding stromal cells rather than *Tsc2*-null myometrial cells. Using flow cytometry and immunofluorescence, we showed increased numbers of G-MDSCs in the blood AND uterus of *Tsc2*-null mice. Immunodepleting MDSCs reduced tumor growth, as did blockade of MDSC recruitment to tumors. Treatment with the NE inhibitor sivelestat phenocopied MDSC immunodepletion, leading to reduced tumor growth. Using two *TSC2*-null cell lines, we confirmed that NE promotes migration, invasion, and proliferation. Thus, our data highlight the importance of NE derived from G-MDSCs and neutrophils in LAM progression, and identify novel therapeutic targets to control LAM tumor growth and invasion.

Materials and methods

Animal studies.

Mouse experiments were performed in accordance with the Care and Use of Laboratory Animals guidelines and approved by the University Committee on Animal Resources at the University of Rochester. Uterine-specific *Tsc2*-null mice (Prizant, et al. 2013) were generated by crossing *Tsc2*-floxed mice with mice expressing *Cre* recombinase driven by the progesterone receptor (*Pgr*) promoter. For xenografts, 6-8-week-old immunocompromised female SCID-NOD mice (Catalog#001803, Jackson Laboratory) were subcutaneously injected with $5x10^6$ ELT3 cells in 0.1 mL of a 1:1 mixture of Matrigel (Corning) and PBS.

Human samples.

De-identified human tissues were handled in accordance with the University Research Subjects Review Board. Tissues were paraffin embedded and processed into 5-micron sections. Sections were deparaffinized and rehydrated for immunofluorescence and hematoxylin and eosin (H&E) staining.

Cell cultures and reagents.

Human *TSC2*-null 621-101 cells from Elizabeth Henske, Brigham and Women's Hospital were derived from a LAM patient's primary angiomyolipoma. Rat *Tsc2*-null ELT3 cells from Cheryl Walker, Texas A&M Health Science Center, were derived from a primary rat leiomyoma. Cells were maintained in DF8 medium incubated in 5% CO_2 in air at 37°C. For *in vitro* experiments, cells were placed in DF8 medium lacking FBS for 24h prior to stimulation with 2.5-5 μg/mL NE (catalog#BML-SE284, ENZO) and 2-10μM sivelestat (catalog#3535, Tocris) for indicated times. Cells were confirmed negative for mycoplasma and bacterial contamination.

Thymidine incorporation assay.

Cell proliferation was analyzed using a 1,5- bromo-2'-deoxyuridine (BrdU) Cell Proliferation Assay Kit (catalog#6813S, Cell Signaling Technology). $1x10^5$ cells per well were plated in 12-well plates in DF8 media followed by a 24h treatment with 5 μg/mL NE in serum-free media. Subsequently, BrdU was added to wells for another 24h. The assay was terminated by fixing cells in 4% paraformaldehyde (Affimetrix) followed by DNA denaturation with 2 N HCl. Cells were blocked with 1.5% normal horse serum (S-2000-20, Vector Labs), and BrdU staining performed according to the manufacturer's instructions. Proliferation rate was assessed by optical density at 450 nm.

Transwell assays.

Tumor cell invasion and migration was evaluated using Transwells. Cells were plated in DF8 media, serum starved for 24h, and detached using trypsin. $5x10^4$ ELT3 or $1x10^5$ 621-101 cells/well for migration and invasion were seeded into the upper chamber containing 8μm pore-size Transwell inserts (Corning) containing serum-free DF8 media with or without NE (2.5ug/mL). 2-10μM sivelestat (as indicated) was used for NE-inhibition. Cells were allowed to migrate to the lower chamber with serum-containing DF8 medium for 12h (ELT3 cells) or

24h (621-101 cells) at 37°C, after which unmigrated cells in the upper chamber were scraped with cotton swabs and cells migrated to the lower side of the membrane were fixed using 4% paraformaldehyde, stained with 1% crystal violet (catalog#45-V5265, Sigma-Aldrich), imaged, and counted using ImageJ (version 1.49) or the PhotoshopCC2018 extended measurement feature. 5 images with the 10X objective were analyzed for each transwell. The same procedure was followed for invasion assays except that transwell inserts were matrigel coated.

Western blotting.

Cells were stimulated with 2.5μg/mL NE for 15-minutes and with 2μM sivelestat at the indicted time points. For total protein, cells were collected and homogenized in RIPA lysis buffer (Pierce) containing protease and phosphatase inhibitors (catalog# PI78440, Thermo Fisher Scientific). Proteins were resolved using 10% SDS-PAGE followed by western blot. Primary antibodies included 1:1,000 anti-phospho-ERK1/2 (catalog#9101, Cell Signaling), 1:1,000 anti-total-ERK1/2 (catalog# 9102, Cell Signaling), and 1:4,000 anti-glyceraldehyde-3-phosphate-dehydrogenase (GAPDH; Cell Signaling).

In vivo treatments.

For Gr-1 depletion, 12-week-old uterine-specific *Tsc2*-null mice were subjected to intraperitoneal injections (i.p.) of 200 mg rat anti-mouse Gr-1 antibody (RB6-8C5, catalog#BE0075, Bio X Cell) or isotype control rat IgG2b antibody (LTF-2, catalog#BE0090, Bio X Cell) twice weekly for 6-weeks. For NE inhibition, 12-week-old mice were administered daily i.p. injections of 5 mg/kg sivelestat (4% DMSO in PBS) or 4% DMSO vehicle. For the CXCR2 inhibition, mice were injected with 1 mg/kg CXCR2-antagonist (SB225002; catalog#2725, Tocris) or 4% DMSO vehicle ip 4-days a week for 6-weeks. Animals were euthanized at 18-weeks of age. Uteri were removed and weighed and subsequently digested for flow cytometry. For histology, paraffin-embedded uterine tissue sections were stained with H&E or indicated antibodies for immunofluorescence. Blood for flow cytometry analysis was collected via retro orbital sinuses or cardiac puncture. Myometrial thickness in longitudinal uterine sections was measured as described (Prizant, et al. 2016). Thickness was measured in three areas from three different sections per experimental or control mouse uteri.

Fluorogenic enzyme activity imaging.

At the experimental end-point, mice were placed on the alfalfa-free diet (Teklad global 16% protein, Envigo) for two-weeks prior to imaging. Mice received 4nmols of a NE-selective optical probe (NE 680 fast; PerkinElmer) in 0.1 mL PBS via tail vein injection. 16h post probe injection, activity was measured using imaging system IVIS Spectrum (PerkinElmer) or in excised tumors using fluorescent microscopy. Signal intensity was imaged and quantified using ImageJ (v1.49).

RNA isolation and quantitative PCR (qPCR).

Total RNA was extracted from mouse uteri using the E.Z.N.A kit (Omega, Norcross, GA, USA) according to manufacturer's instructions. Gene expression was evaluated using qPCR

with mouse *Cxcl5* Taqman primer (Mm00436451_g1). *Cxcl5* mRNA expression level was normalized to housekeeping gene *Gapdh* (Mm99999915_g1) and validated using the ΔΔCt method.

Flow cytometry.

Blood, uteri, and lungs were collected from mice to enumerate MDSCs by flow cytometry using antibodies specific for mouse MDSC markers, Ly6G and Ly6C. Blood, collected in tubes containing heparin, was overlaid on 1-step polymorphs (Catalog#AN221725, Accurate Chemical) to separate white blood cells. Uteri and lungs were digested with collagenase I 6.25 mg/ml (C-7657, Sigma Aldrich) and DNAse 0.295 mg/ml (D-5025-150KU, Sigma Aldrich) to generate single cell suspensions. Residual red blood cells were eliminated with ACK lysis buffer (150 mM NH_4Cl, 10 mM $KHCO_3$, 1 mM Na_2EDTA, pH 7.2). Live cells were counted based on their capacity to exclude trypan blue. Fc receptors on the leukocytes were blocked with 1 μg/ml of rat anti-mouse CD16/CD32 (Fc Block, clone 2.4G, catalog#BE008, BioXCell) for 5-minutes on ice and stained with primary antibodies (0.2 μg/sample): APC rat anti-mouse CD45 (clone 30-F11, catalog#103112, BioLegend), APC-Cy7 rat anti-mouse/human CD11b (clone M1-70, catalog#101226, BioLegend), PE rat anti-mouse Ly6C (clone HK1.4, catalog#12-5932-82, eBioscience), FITC rat anti-mouse Ly6G (clone IA8, catalog#127606, BioLegend). Cells were washed with FACS media (2 % fetal bovine serum and 2.5 mM Na_2EDTA in PBS) and resuspended in FACS media with propidium iodide at 0.5 μg /ml (P4170-25MG, Sigma Aldrich). Samples were collected in a LSRII flow cytometer (BD Biosciences) and analyzed with FlowJo software (10.1r7).

Immunofluorescence.

Human lung tissue sections were deparaffinized and rehydrated in a graded alcohol series. Antigen retrieval was performed in Tris-EDTA buffer pH 8. Sections were incubated with a 1:50 dilution of mouse anti-human CD33 (catalog#133M-15, Sigma-Aldrich) or 1:100 dilution of goat anti-human GPNMB (catalog#AF2550-SP, R&D Biosystems), overnight, at 4°C. On the following day, fluorescein-conjugated anti-mouse or anti-goat antibody (1:200, Vector Laboratories, Burlingame, CA, USA) was used as the secondary antibody and 1 mg/mL Hoechst-33258 (Invitrogen) used for nuclei labeling.

Statistical analysis.

Statistical significance was determined using GraphPad Prism 8.0 software (GraphPad Software, La Jolla, CA). Statistical analysis was performed using standard two-tailed Student's *t*-tests or ordinary one-way ANOVA, considering $p \leq 0.05$ as the threshold for statistical significance.

Results

Neutrophil Elastase (NE) in *Tsc2*-null tumors is stromal in origin

Our previous studies with uterine-specific *Tsc2*-null mice demonstrated significant NE expression and activity in myometrial LAM-like *Tsc2*-null tumors (Prizant, et al. 2016). Since NE is expressed in infiltrating neutrophils or G-MDSCs in other tumor models, rather than in the primary tumor cells themselves (Lerman, et al. 2017), we examined NE activity

and expression in *Tsc2*-null rat ETL3 cell xenografts. *Tsc2*-null rat ELT3 cells were injected into NOD mice. 30-days after inoculation, mice were injected with a NE-specific protease-sensitive fluorescent probe and imaged by IVIS (*in vivo* imaging system). As expected, NE activity was high in tumors (Fig. 1A left mouse, right flank). As a control, we also injected mice with an MMP9-specific protease sensitive fluorescent probe, which demonstrated significant activity (Fig. 1A right mouse, both flanks). To determine whether NE was expressed in ELT3 tumor cells or surrounding infiltrating cells, we performed quantitative PCR on ELT3 cells or several tumors from different mice (see figure legend), using primers recognizing either rat or mouse *NE* (*Elane*) or *Mmp9*. We found that rat ELT3 cells did not express detectable *Elane m*RNA, while *Elane* mRNA in xenografts were exclusively mouse in origin (Fig. 1B). These findings indicated that NE was derived from infiltrating host mouse cells rather than tumor cells themselves. In contrast, both mouse and rat *Mmp9* mRNAs were detected in tumors, and rat *Mmp9* mRNA was expressed in ELT3 cells, confirming that MMP9 originates from both tumor and infiltrating mouse cells.

MDSCs are elevated in uterine-specific *Tsc2*-null mice

Since the NE was expressed in infiltrating mouse cells, and since previous evidence suggests that NE is expressed in MDSCs, we next examined MDSC levels in uterine-specific *Tsc2*-null mice relative to wild-type (WT) littermates. We enumerated MDSCs in the blood, uteri, and lungs by flow cytometry, using antibodies specific for MDSC markers Ly6G and Ly6C, and gated on CD11b. We focused on cells highly expressing both Ly6G and Ly6C, representing primarily G-MDSCs. Notably, to date, there are no definitive cell surface markers to delineate G-MDSCs from neutrophils; thus, in this manuscript, the term G-MDSCs may also include neutrophils, though in general neutrophil levels are thought to be low relative to G-MDSCs in chronic inflammation or cancer (Bronte, et al. 2016). Results showed markedly and significantly increased Ly6G and Ly6C positive G-MDSCs (labeled PMN-MDSC) numbers in the *Tsc2*-knockout (KO) mouse uterus and blood compared to the WT littermate controls (Fig. 2A and B). PMN-MDSCs were also increased in lungs of uterine-specific *Tsc2*-KO animals relative to controls, though the differences were not quite statistically significant with the four mice per group tested. Flow cytometry results were confirmed by immunofluorescent staining for Ly6G in uteri, which demonstrated G-MDSC infiltration across *Tsc2*-null myometrial tumor tissue, compared to WT (Fig. 2C). These results suggest that myometrial tumor formation is likely responsible for mobilization of G-MDSCs from the bone marrow to the periphery and accumulation of G-MDSCs in the uteri of uterine-specific *Tsc2*-null mice. Alternatively, it is possible, though less likely, that the G-MDSC increase is caused by the mouse genotype independent of tumor growth.

MDSC immunodepletion prevents *Tsc2*-null myometrial tumor growth

We next determined whether MDSCs are a marker of *Tsc2*-null tumor burden or whether they directly contribute to tumor progression. Starting at 12-weeks age, we chronically administered uterine-specific *Tsc2*-knockout mice with either anti-Gr1 antibody or a control IgG antibody. After 6-weeks of treatment (18-week old mice), we used flow cytometry of blood to confirm significant immunodepletion of circulating G-MDSCs (Ly6C+/Ly6G+) in anti-Gr1-treated mice relative to knockout mice injected with control antibody (Fig. 3A). We also observed significantly reduced tumor/uterine growth in Gr1-treated versus control-

treated mice, as determined by gross visual estimation (size) and final uterine weights at 18-weeks of age (Fig. 3B&C). Suppression of growth was specific to the smooth muscle cell myometrial layer of the uterus as illustrated by H&E staining of longitudinal uterine sections (Fig. 3D) and quantified by averaging the myometrial layer thickness in various sections from multiple mice (Fig. 3E). These inhibitory effects of MDSC depletion on myometrial tumor growth highlight that MDSCs are not only elevated in response to tumor burden, but also play a critical role in contributing to tumor progression.

Inhibition of MDSC recruitment attenuates *Tsc2*-null myometrial tumor growth

Various chemokines and growth factors produced by tumor cells interact with MDSC cell surface receptors, including CXCR1 and CXCR2, to trigger monocytic and granulocytic MDSC recruitment into tumor sites. Since overall MDSC levels appeared critical for tumor growth, we next determined whether blockade of MDSC recruitment to the tumor bed using a CXCR2 inhibitor, without lowering overall MDSC levels, might similarly reduce *Tsc2*-null myometrial tumor growth.

First, we used quantitative PCR to confirm that *Tsc2*-null uterine tumors in 18-week-old mice expressed mRNA encoding the major CXCR2 ligand, CXCL5. *Cxcl5* mRNA levels were significantly elevated in *Tsc2*-null uterine tumors relative to control normal uteri (Fig. 4A). Furthermore, treatment with a selective CXCR2 antagonist (SB225002) versus control in uterine-specific *Tsc2*-null mice from weeks 12-18 reduced tumor growth (Fig. 4B&C), recapitulating the MDSC depletion study. This suppression of tumor growth was again specific to the myometrial smooth muscle cell layer of the uterus (Fig. 4D&E). Although tumor size and myometrial thickness were reduced by treatment with SB225002, results were slightly less pronounced than when MDSCs were depleted (Fig. 3), suggesting that CXCR2-antagonist treatment was not fully effective. Accordingly, flow cytometric analysis of blood from animals treated with SB225002 or vehicle confirmed no change in overall G-MDSC (Ly6C+/Ly6G+) numbers (Fig. 4G), and a modest but not statistically significant, reduction in G-MDSC numbers in tumors (Fig. 4F). The continued presence of G-MDSCs in tumors indicates that SB225002 was only partially effective in reducing MDSC recruitment to the tumor microenvironment (see discussion). Nevertheless, blockade of CXCR2 receptors in MDSCs significantly reduced tumor growth and myometrial thickness, suggesting that MDSC infiltration into tumors, perhaps in part via CXCL5/CXCR2 interactions, promotes tumor progression.

NE Inhibition by Sivelestat Reduces *Tsc2*-Null Uterine Tumor Growth

Our hypothesis is that one consequence of increased infiltration of MDSCs (primarily granulocytic) could be release of proteolytic enzymes in the tumor microenvironment, eventually leading to metastasis. Given the high expression and activity of NE in *Tsc2*-null myometrial tumors, we postulated that NE might be partially responsible for the pro-tumorigenic effect of MDSCs in tumor progression. In fact, NE is reported to promote tumorigenic phenotypes such as proliferation, epithelial to mesenchymal transition (EMT), migration, invasion, and metastasis in many cancers, though it's role in *Tsc2*-null tumor progression is unknown.

To test our hypothesis, we treated mice with sivelestat, a known inhibitor of NE that is currently approved for human use in some countries (Aikawa and Kawasaki 2014; Aikawa, et al. 2011). We divided KO mice into two groups: sivelestat- and vehicle-treated mice. At the end of the 6-week treatment (from 12-weeks to 18-weeks of age), we observed a slight but not significant difference in circulating G-MDSCs level between the two treatment groups (Fig. 5A&B), which is anticipated as sivelestat should have no effect on overall G-MDSC production and release from bone marrow into circulation. However, unexpectedly, sivelestat significantly blocked G-MDSC infiltration into the tumor site, as analyzed by flow cytometry (Fig. 5C&D), indicating that NE enzyme activity may positively influence the influx of MDSCs into the tumor site.

Importantly, sivelestat substantially reduced uterine tumor growth (Fig. 5E&F), again primarily by reducing myometrial overgrowth and thickening (Fig. 5G&H), phenocopying results from MDSC depletion (Fig. 3). Using the NE-specific fluorescent probe, we confirmed reduction of NE activity within the *Tsc2*-null uteri of sivelestat-versus vehicle-treated mice (Fig. 5I&J). Thus, sivelestat appears to protect mice against the potentially tumor-promoting effects of NE, leading to decelerated tumor growth and reduced G-MDSC influx into the tumor site. Sivelestat administration may therefore be a potential therapeutic strategy to block NE activity and delay progression of tumor development.

NE promotes *Tsc2*-null tumor cell proliferation, migration, and invasion *in vitro*

After establishing that MDSC-derived NE is an important regulator of *Tsc2*-null myometrial growth *in-vivo*, we next focused on specific effects of NE on *Tsc2*-null cell growth *in-vitro*. Previous work showed that NE can promote proliferation, migration, and invasion of tumor cells; thus, we evaluated the effects of NE on these processes in human derived *TSC2*-null 621-101 cells as well as the rat *Tsc2*-null leiomyoma cell line, ELT3. For these studies, we first used dose response and time course assays to determine the lowest dose and time point for NE to induce a near maximum response – these doses and times are shown in the figure legends.

First, using an *in-vitro* transwell migration system, we found that NE enhances migration of *Tsc2*-null rat ELT3 cells relative to untreated cells (Fig. 6A&B). Inhibition of NE enzyme activity with sivelestat abrogated migration. Similarly, we conducted matrigel invasion assays to investigate whether NE treatment supports an invasive behavior in *Tsc2*-null cells. NE modestly increased invasiveness of ELT3 cells through the matrigel membrane relative to control-treated cells (Fig 6C&D). Again, co-treatment with sivelestat abrogated the invasive effects of NE. Third, using BrdU incorporation, we observed an approximate 3-fold increase in proliferation of ELT3 cells by NE (Fig. 6F). Finally, to begin investigating the mechanisms underlying NE-mediated effects on *Tsc2*-null tumor progression, we examined the influence of NE on Erk1/2 activation. Exposing ELT3 cells to NE for 15-minutes induced Erk1/2 phosphorylation relative to vehicle-treated cells (Fig. 6B). Sivelestat attenuated NE-induced Erk1/2 phosphorylation, indicating that, as in the migration and invasion studies, NE's catalytic activity is required for rapid activation of Erk phosphorylation. Notably, we observed what appears to be NE-induced degradation of tErk protein. NE is known to be internalized by some target cells (Houghton, et al. 2010;

Mantovani, et al. 2011), which may explain this observation. Further studies are underway to better understand these effects.

Studies on the effects of NE on proliferation, migration and invasion, and MAPK activation in human *TSC2*-null 621-101 cells demonstrated similar results, though with less consistent inhibition with sivelestat in every assay, recapitulating that NE activity is positively linked to facilitating cell proliferation, invasion and migration, as well as MAPK signaling (Supplementary Fig. 1).

MDSCs are dispersed throughout human LAM lung tissue but not healthy controls

After confirming that MDSCs are present and promoting tumor growth in mouse models, we next examined whether MDSCs were present in human lung biopsies from patients with LAM. We performed immunofluorescence on serial lung sections from LAM patients versus healthy individuals to detect the expression of CD33, a common human myeloid cell marker (Fig. 7). As a marker for LAM cells, we stained adjacent sections from the same lungs with an antibody directed against the melanocytic marker GPNMB (Prizant, et al. 2016; Rose, et al. 2010). Our results depicted strong and diffuse CD33 staining in the samples from LAM patients (Fig. 7B, red). Neither CD33 (Fig. 7A) nor GPNMB staining (not shown) (Prizant, et al. 2016; Taya and Hammes 2018) were detected in tissue from healthy lungs, validating selective infiltration of myeloid cells into the lungs of LAM patients and suggesting that local lung myeloid cells, including MDSCs, might be promoting tumor growth and progression.

Discussion

NE is a serine protease secreted by granulocytic cells that degrades phagocytosed foreign microorganisms; thus playing a protective role in host defense against infection (Mantovani, et al. 2011). However, NE actions are upregulated with chronic inflammation caused by a variety of conditions, including trauma, interstitial lung disease, pulmonary fibrosis, and cancer. Increased NE concentration in tumors is associated with late-stage disease and poor survival (Lerman and Hammes 2018).

Here we demonstrated that NE regulates growth in a mouse model for LAM tumors. We previously showed that *NE* mRNA expression and NE activity were elevated in *Tsc2*-null mouse myometrial tumors (Prizant, et al. 2016). Here we found that *in-vivo* inhibition of NE with the antagonist sivelestat markedly reduced tumor growth and myometrial proliferation (Fig. 3). Using two *TSC2*-null cell lines, NE promoted proliferation, migration, and invasion, as well as rapid activation of MAPK signaling (Fig. 6 and Sup. Fig. 1). Secreted proteases modulate pro-proliferative and pro-metastatic signaling cascades in cancer cells by activating kinases, cell surface receptors, chemokines, and other growth factors. For example, NE triggers release of TGF-β and transactivation of cell surface receptors EGFR and TLR4 to promote proliferation and migration (Houghton, et al. 2010; Wada, et al. 2007). In addition, NE internalization can directly induce tumor cell proliferation by entering endosomes and cleaving insulin receptor substrate-1, which increases phosphatidylinositol 3-kinase activity to promote proliferation (Houghton, et al. 2010; Mantovani, et al. 2011). In

fact, endosomal NE is necessary for proliferation, as blocking endosome formation prevented proliferation (Gregory, et al. 2012).

Interestingly, the *Tsc2*-null ELT3 rat uterine cell line expressed no detectable *NE* mRNA by quantitative PCR (Fig. 1), nor did rat ELT3 xenografts in mice (Fig. 1). In contrast, xenografts expressed mouse mRNA encoding NE. These findings suggest that the NE activity in *Tsc2*-null xenografts and *Tsc2*-null uterine tumors comes from surrounding stromal cells rather than *Tsc2*-null tumor cells. With this in mind, we investigated the role of MDSCs in the progression of LAM-like tumors. MDSCs are a heterogeneous population of pro-inflammatory cells infiltrating tumor stroma, and NE expression in G-MDSCs is upregulated in tumor bearing mice compared to naïve mice (Youn, et al. 2012). While MDSCs function in part by suppressing T-cells to allow tumor growth, MDSCs also directly stimulate tumor growth independent of T-cell suppression (Lerman, et al. 2017; Marvel and Gabrilovich 2015). Since NE is expressed in G-MDSCs, and given the potential role of NE in promoting cancer progression, we examined the role of MDSCs in our uterine-specific *Tsc2*-null mouse model for LAM. We found elevated G-MDSC levels in the blood, uterus, and lungs of uterine-specific *Tsc2*-null mice relative to controls. Furthermore, resembling NE inhibition with sivelestat, immunodepletion of MDSCs in this mouse model ameliorated myometrial tumor growth.

Tumor cells secrete chemokines that interact with cell surface MDSC receptors such as CXCR1/2 to promote MDSC migration into tumor sites (Houghton 2010; Marvel and Gabrilovich 2015). Accordingly, the CXCR1/2 ligand CXCL5 was upregulated in *Tsc2*-null myometrial tumors (Fig. 4A). Blockade of CXCR2 receptors with SB225002 to prevent MDSC recruitment significantly reduced myometrial tumor growth, although not to the same extent as MDSC immunodepletion (Fig. 4). This lesser effect of SB225002 was likely due to limited efficacy in reducing MDSC recruitment, as we observed only slight reduction in infiltrating MDSC levels within myometrial tumors, possibly due to CXCR1 compensating for the SB225002's antagonistic effect on CXCR2. Notably, other tumor models demonstrate a critical role for CXCR2 as a modulator of neutrophil attraction. In a K-ras mouse model of lung cancer (CC-LR), CXCR2 inhibition suppressed neutrophil recruitment into lungs and reduced tumor volume. Crossing CC-LR mice with NE knockout mice also inhibited lung cancer development (Gong, et al. 2013), again emphasizing the connection between MDSCs and NE. It is also possible that CXCR2 is expressed on tumor cells and autocrine CXCL5/CXCR2 signaling is occurring to partially promote tumor growth.

Surprisingly, sivelestat-mediated inhibition of NE markedly reduced G-MDSC influx into *Tsc2*-null tumor sites, but did not affect G-MDSC numbers in blood (Fig. 5). Perhaps this is due to impairment of tumor growth, which negatively influences chemokine production. Alternatively, NE can activate chemokines, cytokines, and other growth factors that promote MDSC chemotaxis to tumor microenvironments (Chua and Laurent 2006); thus inhibition of NE might indirectly reduce MDSC infiltration. Interestingly, NE cleaves and inactivates G-CSF and its receptor (El Ouriaghli, et al. 2003; Piper, et al. 2010). G-CSF promotes granulocytic-MDSC production from bone marrow (Abrams and Waight 2012; Waight, et al. 2011); thus, NE-mediated degradation of G-CSF and its receptors might partially attenuate

G-MDSCs production. In sivelestat-treated mice, G-CSF–stimulated granulopoiesis would no longer be suppressed by NE, perhaps explaining why we see no reduction of blood MDSC levels (Fig. 5B, D).

NE appears to be particularly important in promoting tumor growth in lungs. In addition to suppressive effects of NE in murine lung tumors, single nucleotide polymorphisms in the promoter of the *NE* gene were associated with higher risks of lung cancer (Taniguchi, et al. 2002). Furthermore, deficiency of alpha-1-antitrypsin, a natural NE inhibitor, is associated with an increased risk of developing lung cancer (Sun and Yang 2004; Yang, et al. 2005), suggesting that the balance between NE and inhibitors may contribute to tumor growth in the lungs.

In addition to direct effects on tumor growth and metastasis, NE may facilitate tumor progression in lungs through indirect means. NE degrades elastin as well as collagens, cadherins, fibronectins, and proteoglycans (Chua and Laurent 2006) perhaps allowing tumors to invade lung tissue. Direct NE-mediated lung destruction can also cause air trapping, leading to longer carcinogen exposure, degradation of matrix proteins, and activation of tumor-necrosis-factor (TNF) signaling (Chua and Laurent 2006). Thus, MDSC recruitment into the lungs, followed by NE release, may do more than promote LAM tumor cell growth – it may contribute to the destructive lung process culminating into cyst formation.

In conclusion, we propose that *Tsc2*-null tumors secrete chemokines such as CXCL5, which orchestrate MDSC infiltration into the tumor microenvironment. Once there, NE secretion likely from G-MDSCs facilitates tumor growth, migration and invasion. This is may be happening in TSC2-null tumors throughout the body of LAM patients, and may contribute to metastasis to the lungs. Once within the lungs, NE likely both promotes tumor growth and contributes to lung destruction (Fig. 8). Therefore, targeting NE activity or G-MDSC function present as rational approaches toward treating patients with LAM.

Supplementary Material

Refer to Web version on PubMed Central for supplementary material.

Acknowlegements

We thank Amanda Wahl for assistance in optimizing *in-vitro* NE treatment conditions; Christina Seger and Michael Sellix for technical assistance with *in-vivo* therapies; and Elaine Smolock for editorial assistance with the manuscript. We also thank Patricia Sime for providing human lung samples and Thomas Colby (Mayo, Phoenix) for providing human LAM samples.

Funding

This work was supported by NIH grant R01 CA193583.

References

Abrams SI & Waight JD 2012 Identification of a G-CSF-Granulocytic MDSC axis that promotes tumor progression. Oncoimmunology 1 550–551. [PubMed: 22754783]

Aikawa N & Kawasaki Y 2014 Clinical utility of the neutrophil elastase inhibitor sivelestat for the treatment of acute respiratory distress syndrome. Ther Clin Risk Manag 10 621–629. [PubMed: 25120368]

Aikawa N, Ishizaka A, Hirasawa H, Shimazaki S, Yamamoto Y, Sugimoto H, Shinozaki M, Taenaka N, Endo S, Ikeda T, et al. 2011 Reevaluation of the efficacy and safety of the neutrophil elastase inhibitor, Sivelestat, for the treatment of acute lung injury associated with systemic inflammatory response syndrome; a phase IV study. Pulm Pharmacol Ther 24 549–554. [PubMed: 21540122]

Alfaro C, Teijeira A, Onate C, Perez G, Sanmamed MF, Andueza MP, Alignani D, Labiano S, Azpilikueta A, Rodriguez-Paulete A, et al. 2016 Tumor-Produced Interleukin-8 Attracts Human Myeloid-Derived Suppressor Cells and Elicits Extrusion of Neutrophil Extracellular Traps (NETs). Clin Cancer Res 22 3924–3936. [PubMed: 26957562]

Ando K, Kurihara M, Kataoka H, Ueyama M, Togo S, Sato T, Doi T, Iwakami S, Takahashi K, Seyama K, et al. 2013 Efficacy and safety of low-dose sirolimus for treatment of lymphangioleiomyomatosis. Respir Investig 51 175–183.

Bittmann I, Rolf B, Amann G & Lohrs U 2003 Recurrence of lymphangioleiomyomatosis after single lung transplantation: new insights into pathogenesis. Hum Pathol 34 95–98. [PubMed: 12605373]

Bronte V, Brandau S, Chen SH, Colombo MP, Frey AB, Greten TF, Mandruzzato S, Murray PJ, Ochoa A, Ostrand-Rosenberg S, et al. 2016 Recommendations for myeloid-derived suppressor cell nomenclature and characterization standards. Nat Commun 7 12150. [PubMed: 27381735]

Carsillo T, Astrinidis A & Henske EP 2000 Mutations in the tuberous sclerosis complex gene TSC2 are a cause of sporadic pulmonary lymphangioleiomyomatosis. Proc Natl Acad Sci U S A 97 6085–6090. [PubMed: 10823953]

Chua F & Laurent GJ 2006 Neutrophil elastase: mediator of extracellular matrix destruction and accumulation. Proc Am Thorac Soc 3 424–427. [PubMed: 16799086]

Dumitru CA, Lang S & Brandau S 2013 Modulation of neutrophil granulocytes in the tumor microenvironment: mechanisms and consequences for tumor progression. Semin Cancer Biol 23 141–148. [PubMed: 23485549]

Dumitru CA, Moses K, Trellakis S, Lang S & Brandau S 2012 Neutrophils and granulocytic myeloid-derived suppressor cells: immunophenotyping, cell biology and clinical relevance in human oncology. Cancer Immunol Immunother 61 1155–1167. [PubMed: 22692756]

El Ouriaghli F, Fujiwara H, Melenhorst JJ, Sconocchia G, Hensel N & Barrett AJ 2003 Neutrophil elastase enzymatically antagonizes the in vitro action of G-CSF: implications for the regulation of granulopoiesis. Blood 101 1752–1758. [PubMed: 12393522]

El Rayes T, Catena R, Lee S, Stawowczyk M, Joshi N, Fischbach C, Powell CA, Dannenberg AJ, Altorki NK, Gao D, et al. 2015 Lung inflammation promotes metastasis through neutrophil protease-mediated degradation of Tsp-1. Proc Natl Acad Sci U S A 112 16000–16005. [PubMed: 26668367]

Ferrans VJ, Yu ZX, Nelson WK, Valencia JC, Tatsuguchi A, Avila NA, Riemenschn W, Matsui K, Travis WD & Moss J 2000 Lymphangioleiomyomatosis (LAM): a review of clinical and morphological features. J Nippon Med Sch 67 311–329. [PubMed: 11031360]

Gabrilovich DI, Ostrand-Rosenberg S & Bronte V 2012 Coordinated regulation of myeloid cells by tumours. Nat Rev Immunol 12 253–268. [PubMed: 22437938]

Galdiero MR, Varricchi G, Loffredo S, Mantovani A & Marone G 2018 Roles of neutrophils in cancer growth and progression. J Leukoc Biol 103 457–464. [PubMed: 29345348]

Gong L, Cumpian AM, Caetano MS, Ochoa CE, De la Garza MM, Lapid DJ, Mirabolfathinejad SG, Dickey BF, Zhou Q & Moghaddam SJ 2013 Promoting effect of neutrophils on lung tumorigenesis is mediated by CXCR2 and neutrophil elastase. Molecular cancer 12 154–154. [PubMed: 24321240]

Gregory AD, Hale P, Perlmutter DH & Houghton AM 2012 Clathrin pit-mediated endocytosis of neutrophil elastase and cathepsin G by cancer cells. J Biol Chem 287 35341–35350. [PubMed: 22915586]

Grosse-Steffen T, Giese T, Giese N, Longerich T, Schirmacher P, Hansch GM & Gaida MM 2012 Epithelial-to-mesenchymal transition in pancreatic ductal adenocarcinoma and pancreatic tumor

cell lines: the role of neutrophils and neutrophil-derived elastase. Clin Dev Immunol 2012 720768. [PubMed: 23227088]

Hayashi T, Kumasaka T, Mitani K, Terao Y, Watanabe M, Oide T, Nakatani Y, Hebisawa A, Konno R, Takahashi K, et al. 2011 Prevalence of uterine and adnexal involvement in pulmonary lymphangioleiomyomatosis: a clinicopathologic study of 10 patients. Am J Surg Pathol 35 1776–1785. [PubMed: 22020043]

Ho A-S, Chen C-H, Cheng C-C, Wang C-C, Lin H-C, Luo T-Y, Lien G-S & Chang J 2014 Neutrophil elastase as a diagnostic marker and therapeutic target in colorectal cancers. Oncotarget 5 473–480. [PubMed: 24457622]

Houghton AM 2010 The paradox of tumor-associated neutrophils: fueling tumor growth with cytotoxic substances. Cell Cycle 9 1732–1737. [PubMed: 20404546]

Houghton AM, Rzymkiewicz DM, Ji H, Gregory AD, Egea EE, Metz HE, Stolz DB, Land SR, Marconcini LA, Kliment CR, et al. 2010 Neutrophil elastase-mediated degradation of IRS-1 accelerates lung tumor growth. Nat Med 16 219–223. [PubMed: 20081861]

Karbowniczek M, Astrinidis A, Balsara BR, Testa JR, Lium JH, Colby TV, McCormack FX & Henske EP 2003 Recurrent lymphangiomyomatosis after transplantation: genetic analyses reveal a metastatic mechanism. Am J Respir Crit Care Med 167 976–982. [PubMed: 12411287]

Kelly J & Moss J 2001 Lymphangioleiomyomatosis. Am J Med Sci 321 17–25. [PubMed: 11202475]

Krymskaya VP 2008 Smooth muscle-like cells in pulmonary lymphangioleiomyomatosis. Proc Am Thorac Soc 5 119–126. [PubMed: 18094094]

Lerman I & Hammes SR 2018 Neutrophil elastase in the tumor microenvironment. Steroids 133 96–101. [PubMed: 29155217]

Lerman I, Garcia-Hernandez ML, Rangel-Moreno J, Chiriboga L, Pan C, Nastiuk KL, Krolewski JJ, Sen A & Hammes SR 2017 Infiltrating Myeloid Cells Exert Protumorigenic Actions via Neutrophil Elastase. Mol Cancer Res 15 1138–1152. [PubMed: 28512253]

Mantovani A, Cassatella MA, Costantini C & Jaillon S 2011 Neutrophils in the activation and regulation of innate and adaptive immunity. Nat Rev Immunol 11 519–531. [PubMed: 21785456]

Marvel D & Gabrilovich DI 2015 Myeloid-derived suppressor cells in the tumor microenvironment: expect the unexpected. J Clin Invest 125 3356–3364. [PubMed: 26168215]

McCormack FX 2006 Lymphangioleiomyomatosis. MedGenMed 8 15.

McCormack FX, Inoue Y, Moss J, Singer LG, Strange C, Nakata K, Barker AF, Chapman JT, Brantly ML, Stocks JM, et al. 2011 Efficacy and safety of sirolimus in lymphangioleiomyomatosis. N Engl J Med 364 1595–1606. [PubMed: 21410393]

Piper MG, Massullo PR, Loveland M, Druhan LJ, Kindwall-Keller TL, Ai J, Copelan A & Avalos BR 2010 Neutrophil elastase downmodulates native G-CSFR expression and granulocyte-macrophage colony formation. J Inflamm (Lond) 7 5. [PubMed: 20205821]

Prizant H, Sen A, Light A, Cho SN, DeMayo FJ, Lydon JP & Hammes SR 2013 Uterine-specific loss of Tsc2 leads to myometrial tumors in both the uterus and lungs. Mol Endocrinol 27 1403–1414. [PubMed: 23820898]

Prizant H, Taya M, Lerman I, Light A, Sen A, Mitra S, Foster TH & Hammes SR 2016 Estrogen maintains myometrial tumors in a lymphangioleiomyomatosis model. Endocr Relat Cancer 23 265–280. [PubMed: 26880751]

Rose AA, Grosset AA, Dong Z, Russo C, Macdonald PA, Bertos NR, St-Pierre Y, Simantov R, Hallett M, Park M, et al. 2010 Glycoprotein nonmetastatic B is an independent prognostic indicator of recurrence and a novel therapeutic target in breast cancer. Clin Cancer Res 16 2147–2156. [PubMed: 20215530]

Smolarek TA, Wessner LL, McCormack FX, Mylet JC, Menon AG & Henske EP 1998 Evidence that lymphangiomyomatosis is caused by TSC2 mutations: chromosome 16p13 loss of heterozygosity in angiomyolipomas and lymph nodes from women with lymphangiomyomatosis. Am J Hum Genet 62 810–815. [PubMed: 9529362]

Sun Z & Yang P 2004 Role of imbalance between neutrophil elastase and α1-antitrypsin in cancer development and progression. The Lancet Oncology 5 182–190. [PubMed: 15003202]

Taniguchi K, Yang P, Jett J, Bass E, Meyer R, Wang Y, Deschamps C & Liu W 2002 Polymorphisms in the promoter region of the neutrophil elastase gene are associated with lung cancer development. Clin Cancer Res 8 1115–1120. [PubMed: 11948122]

Taveira-Dasilva AM, Rabel A, Gochuico BR, Avila NA & Moss J 2011 Prevalence of uterine leiomyomas in lymphangioleiomyomatosis. Fertil Steril 96 711–714 e711. [PubMed: 21880281]

Taya M & Hammes SR 2018 Glycoprotein Non-Metastatic Melanoma Protein B (GPNMB) and Cancer: A Novel Potential Therapeutic Target. Steroids 133 102–107. [PubMed: 29097143]

Vaguliene N, Zemaitis M, Lavinskiene S, Miliauskas S & Sakalauskas R 2013 Local and systemic neutrophilic inflammation in patients with lung cancer and chronic obstructive pulmonary disease. BMC Immunol 14 36. [PubMed: 23919722]

Wada Y, Yoshida K, Tsutani Y, Shigematsu H, Oeda M, Sanada Y, Suzuki T, Mizuiri H, Hamai Y, Tanabe K, et al. 2007 Neutrophil elastase induces cell proliferation and migration by the release of TGF-alpha, PDGF and VEGF in esophageal cell lines. Oncol Rep 17 161–167. [PubMed: 17143494]

Waight JD, Hu Q, Miller A, Liu S & Abrams SI 2011 Tumor-derived G-CSF facilitates neoplastic growth through a granulocytic myeloid-derived suppressor cell-dependent mechanism. PLoS One 6 e27690. [PubMed: 22110722]

Wang G, Lu X, Dey P, Deng P, Wu CC, Jiang S, Fang Z, Zhao K, Konaparthi R, Hua S, et al. 2016 Targeting YAP-Dependent MDSC Infiltration Impairs Tumor Progression. Cancer Discov 6 80–95. [PubMed: 26701088]

Yamashita J, Ogawa M, Abe M, Hayashi N, Kurusu Y, Kawahara K & Shirakusa T 1997 Tumor neutrophil elastase is closely associated with the direct extension of non-small cell lung cancer into the aorta. Chest 111 885–890. [PubMed: 9106565]

Yang P, Bamlet WR, Sun Z, Ebbert JO, Aubry MC, Krowka MJ, Taylor WR, Marks RS, Deschamps C, Swensen SJ, et al. 2005 Alpha1-antitrypsin and neutrophil elastase imbalance and lung cancer risk. Chest 128 445–452. [PubMed: 16002971]

Youn JI, Collazo M, Shalova IN, Biswas SK & Gabrilovich DI 2012 Characterization of the nature of granulocytic myeloid-derived suppressor cells in tumor-bearing mice. J Leukoc Biol 91 167–181. [PubMed: 21954284]

Zhou J, Nefedova Y, Lei A & Gabrilovich D 2018 Neutrophils and PMN-MDSC: Their biological role and interaction with stromal cells. Semin Immunol 35 19–28. [PubMed: 29254756]

A.

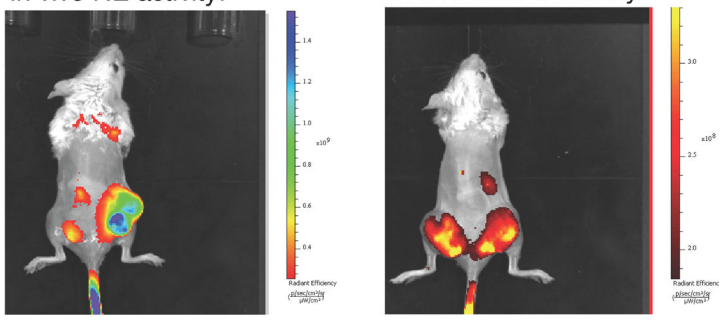

B.

	Rat ELT3 Xenograft Tumors	Rat ELT3 Cell line
Rat *Elane*	ND	ND
Mouse *Elane*	32.6±0.1.23 (13.3±0.88)	ND
	Rat ELT3 Xenograft Tumors	Rat ELT3 Cell line
Rat *Mmp9*	28.72 (12.30)	31.96 (13.36)
Mouse *Mmp9*	24.21 (5.40)	ND

Figure 1. Neutrophil Elastase (NE) in Tsc2-null tumors is stromal in origin.

A. Intratumoral NE activity was measured using NE-specific (left mouse) or MMP-specific (right mouse) optical probes in immunocompromised SCID-NOD mice bearing *Tsc2*-null rat ELT3 xenografts. Tumors were injected bilaterally in both mice but only one tumor grew in the left mouse. ELT3 xenografts expressed elevated NE activity (left). As a positive control, tumors also expressed high MMP activity (right). B. *Elane* (NE) and *MMP9* mRNA expressions were measured by quantitative PCR using rat or mouse specific primers in rat ELT3 xenografts. Rat and mouse *Elane* and *MMP9* mRNA expressions are quantified relative to rat and mouse, respectively, *B2m* mRNA expression. N=4 xenografts from 2 mice for *Elane* and n=2 xenografts each from 2 different mice for *MMP9*. Average Ct values are shown (±SD for *Elane*) with average ΔCt (±SD for *Elane*) in parentheses). ND=not detected.

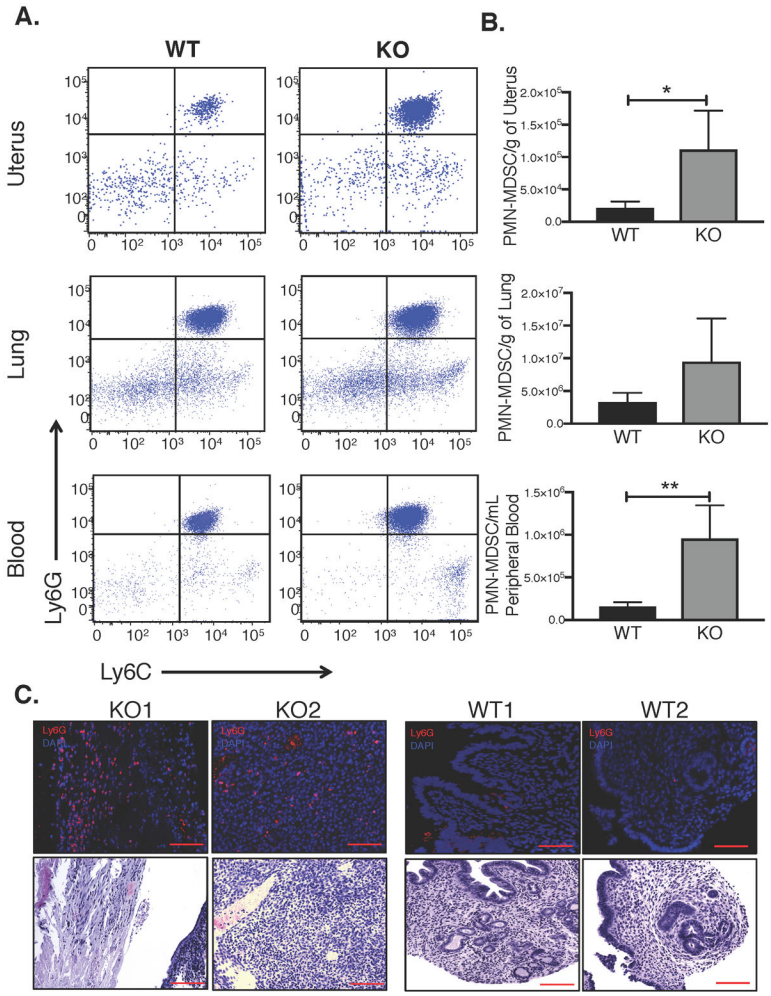

Figure 2. MDSCs levels are elevated in uterine-specific Tsc2-null mice.

A. Representative dot plots of granulocytic, or PMN-MDSC levels in blood and organs of 18-week old KO vs. WT mice. Dot plots depict Ly6G versus Ly6C expression gated on CD11b live cells in uterus, lung, and peripheral blood. B. PMN-MDSCs (Ly6C+/Ly6G+) in uterus, lung and peripheral blood were quantified in KO mice relative to WT mice and analyzed using unpaired two-tailed t test (n=4/group, *p<0.05, **p<0.01). C. Representative immunofluorescence staining for Ly6G (infiltrating PMN-MDSCs) and adjacent H&E stains in KO vs. WT mice is shown (top; scale bar, 100μm) and corresponding H&E staining on serial sections (bottom; scale bar, 100μm).

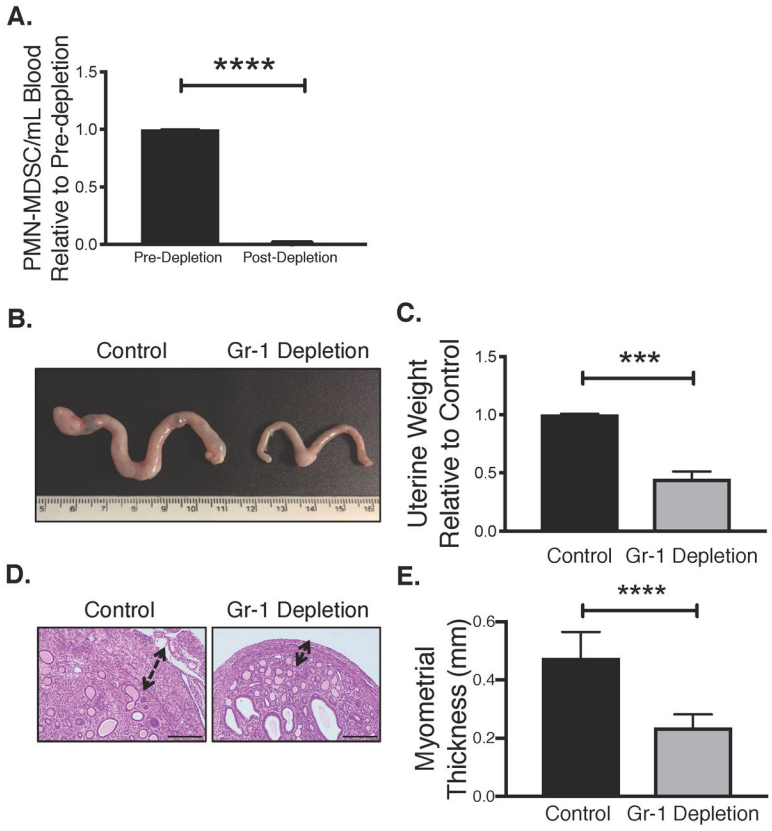

Figure 3. MDSC immunodepletion reduces Tsc2-null myometrial tumor growth.

A. Peripheral blood PMN-MDSCs were assessed by flow cytometry in KO mice 6 weeks after initiation of isotype control or Gr-1 antibody treatment. Statistical significance was analyzed using unpaired two-tailed t test (n=3/treatment group, ****p<0.0001). B. Representative uterine tumor growth from both groups. C. Uterine weights were compared between isotype control and Gr-1 depletion groups using unpaired two-tailed t test (n=3/treatment group, ***p<0.001). Data are expressed as uterine weight relative to matched control-treated mice. D. Representative H&E depicting myometrial thickness in isotype control and Gr1-depleted mice (scale bar, 100μm). E. Myometrial thickness was measured in isotype control and Gr1-depleted mice and analyzed using unpaired two-tailed t test (n=3/treatment group, ****p<0.0001).

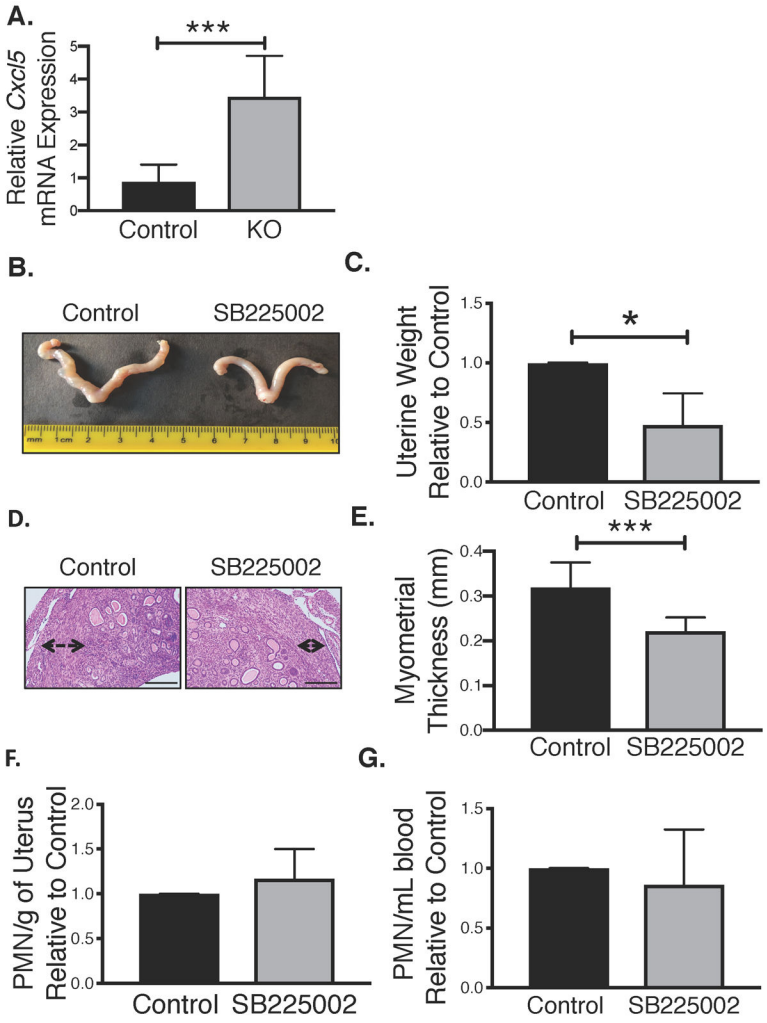

Figure 4. Inhibition of MDSC recruitment attenuates Tsc2-null myometrial tumor growth.

A. Analysis of *Cxcl5* expression relative to *GAPDH* in KO and control mice by quantitative PCR, using unpaired two-tailed t test (n=8/control group; n=6/KO group, ***p<0.001) B. Representative images of uterine tumor growth from control and CXCR2-antagonist (1mg/mL, SB225002) groups. C. Uterine weight was compared between control and CXCR2-antagonist treated groups using unpaired two-tailed t test (n=4/treatment group, *p<0.05). Data are shown as uterine weight relative to matched control treated mice. D. Representative H&E depicting myometrial thickness in control and CXCR2-antagonist treated mice (scale bar, 100μm). E. Myometrial thickness was quantified in control and CXCR2-antagonist treated mice using unpaired two-tailed t test (n=4/treatment group, ***p<0.001). F. Tumor-infiltrating PMN-MDSCs were assessed by flow cytometry in control and CXCR2 antagonist treatment groups after 6 weeks of treatment (n=4/treatment group). Data are shown as PMN-MDSCs per gram of uterus relative to matched controls. G. Circulating PMN-MDSCs levels in CXCR2-anatonist treated mice were quantified relative to control using unpaired two-tailed t test (n=4 separate studies).

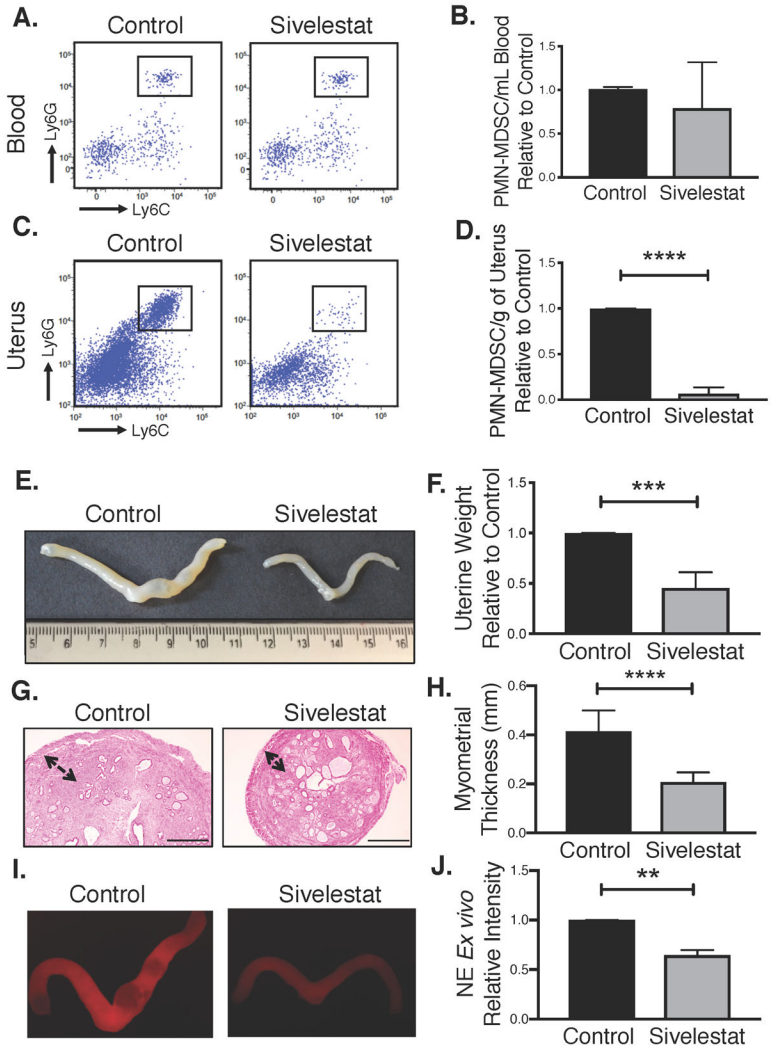

Figure 5. Direct NE inhibition by sivelestat reduces Tsc2-null uterine tumor growth.

A. Representative flow cytometry plots showing $Ly6G^+/Ly6C^+$ cells in peripheral blood of control and sivelestat treated mice. B. The relative number of PMN-MDSCs in peripheral blood of treated compared to control mice was analyzed using unpaired two-tailed t test (n=4, $p>0.05$). C. Representative flow cytometry plots showing $Ly6G^+/Ly6C^+$ cells in tumors of sivelestat relative to control treated mice. D. The number of PMN-MDSCs in uteri of treatment mice relative to control mice was analyzed using unpaired two-tailed t test (n=3, ****$p<0.0001$). E. Representative images of uterine tumor growth from both groups. F. Uterine weights were compared between control and sivelestat treated groups using unpaired two-tailed t test (n=3, ***$p<0.001$,). Data are shown as uterine tumor weight relative to matched control treated animals. G. Representative H&E depicting myometrial thickness in control and sivelestat treated mice (scale bar, 100μm). H. Myometrial thickness was measured in control and sivelestat treated mice and quantified using unpaired two-tailed t test (n=3, ****$p<0.0001$). I. Representative fluorescent images of intratumoral NE activity measured *ex vivo* using intravenous administration of a NE-specific optical probe to control and sivelestat treated mice. J. Intratumor NE activity was quantified using ImageJ. Data

represent signals in sivelestat-treated mice relative to matched control treated. Data are analyzed using unpaired two-tailed t test (n=3 separate studies, $**p<0.01$).

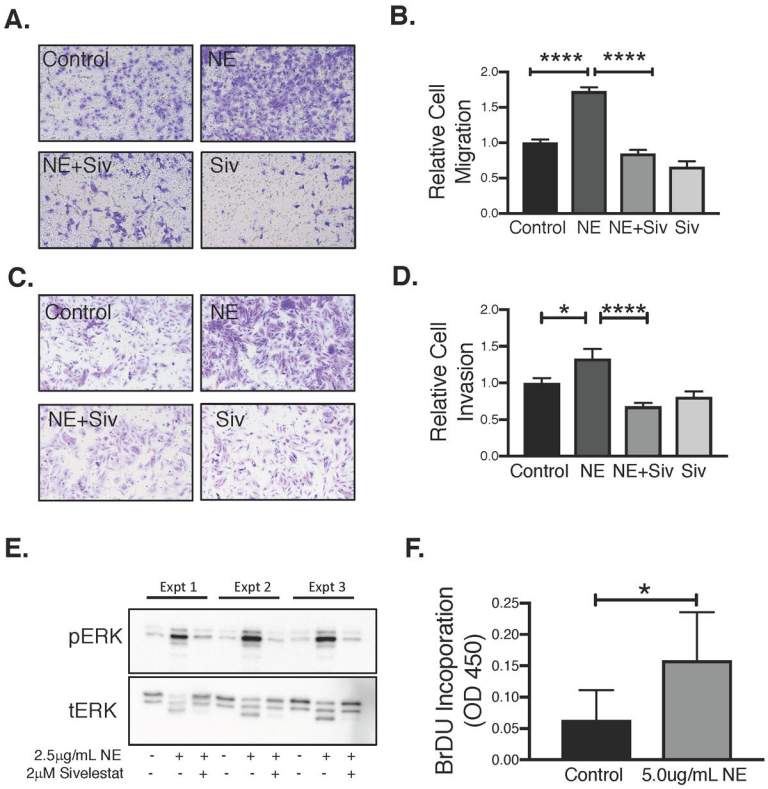

Figure 6. NE promotes rat myometrial TSC2-null tumor migration, invasion, and proliferation in vitro.

A. Rat *Tsc2*-null ELT3 cells were serum starved and transferred into 8-μm uncoated transwells in the presence of NE (2.5μg/mL) or vehicle. Migration of cells toward a chemotactic medium with 10% FBS was measured after 24 hours. Representative images shown. B. Relative number of migrated ELT3 cells was quantified using PhotoshopCC2018 extended measurement feature and analyzed by ANOVA (n=3, ****p<0.0001). C. ELT3 cells were serum starved and transferred into 8-μm Matrigel-transwells in the presence of NE (2.5μg/mL) or vehicle plus or minus sivelestat (10 μM). Invasion of cells toward a chemotactic medium with 10% FBS was measured after 24 hours. Representative images shown. D. Relative number of invaded ELT3 cells was quantified and analyzed as above (n=4, *p<0.05, ****p<0.0001). E. NE activates MAPK signaling. Rat *Tsc2*-null ELT3 cells were serum starved and treated with NE (2.5μg/mL) for 15 minutes, or in the presence of 2 μM sivelestat or vehicle. pERK1/2 and tERK1/2 phosphorylation were examined by Western blot. Three experiments shown. F. Rat *Tsc2*-null ELT3 cells were serum-starved prior to NE (2.5 μg/mL) treatment for 24 hours. Proliferation was examined by BrdU incorporation and relative change in proliferation between treated and untreated samples was analyzed by unpaired two-tailed t test (n=4, *p<0.05).

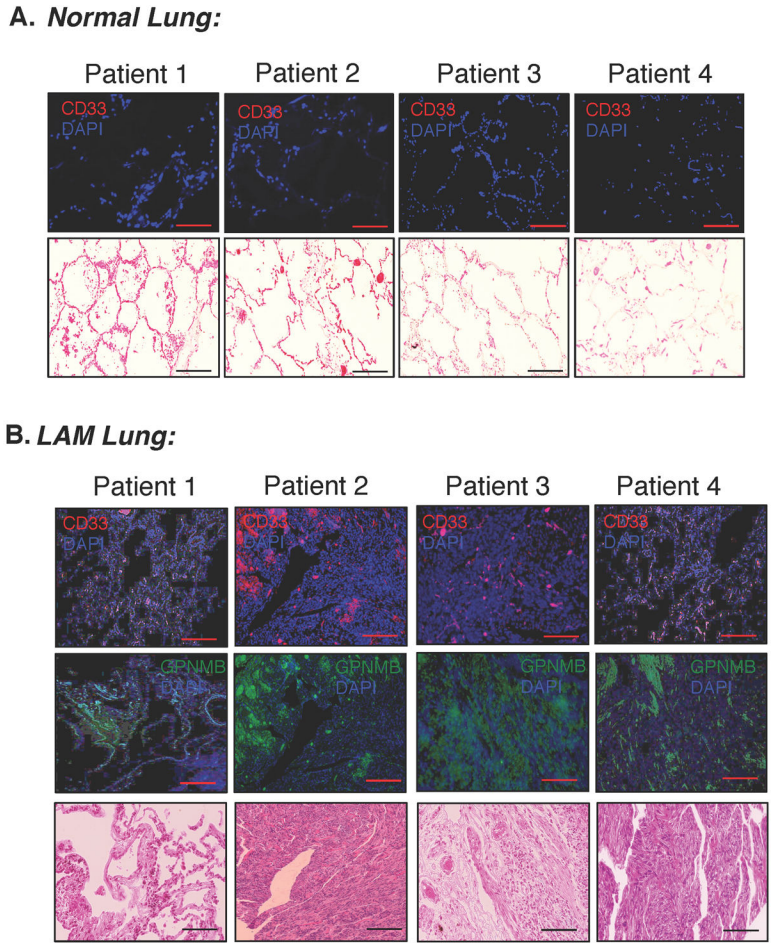

Figure 7. MDSCs are dispersed throughout human LAM lung tissue but not normal controls.

A. Representative immunofluorescent stains for CD33 (infiltrating MDSCs) in four different normal lung tissue sections, and eosin staining from adjacent sections (scale bar, 100μm). B. Representative immunofluorescent stains on adjacent sections for GPNMB protein (green, marker for LAM) and CD33 (red, infiltrating MDSCs) in four different human LAM patient lung tissues as well as eosin staining from adjacent sections (scale bar, 100μm).

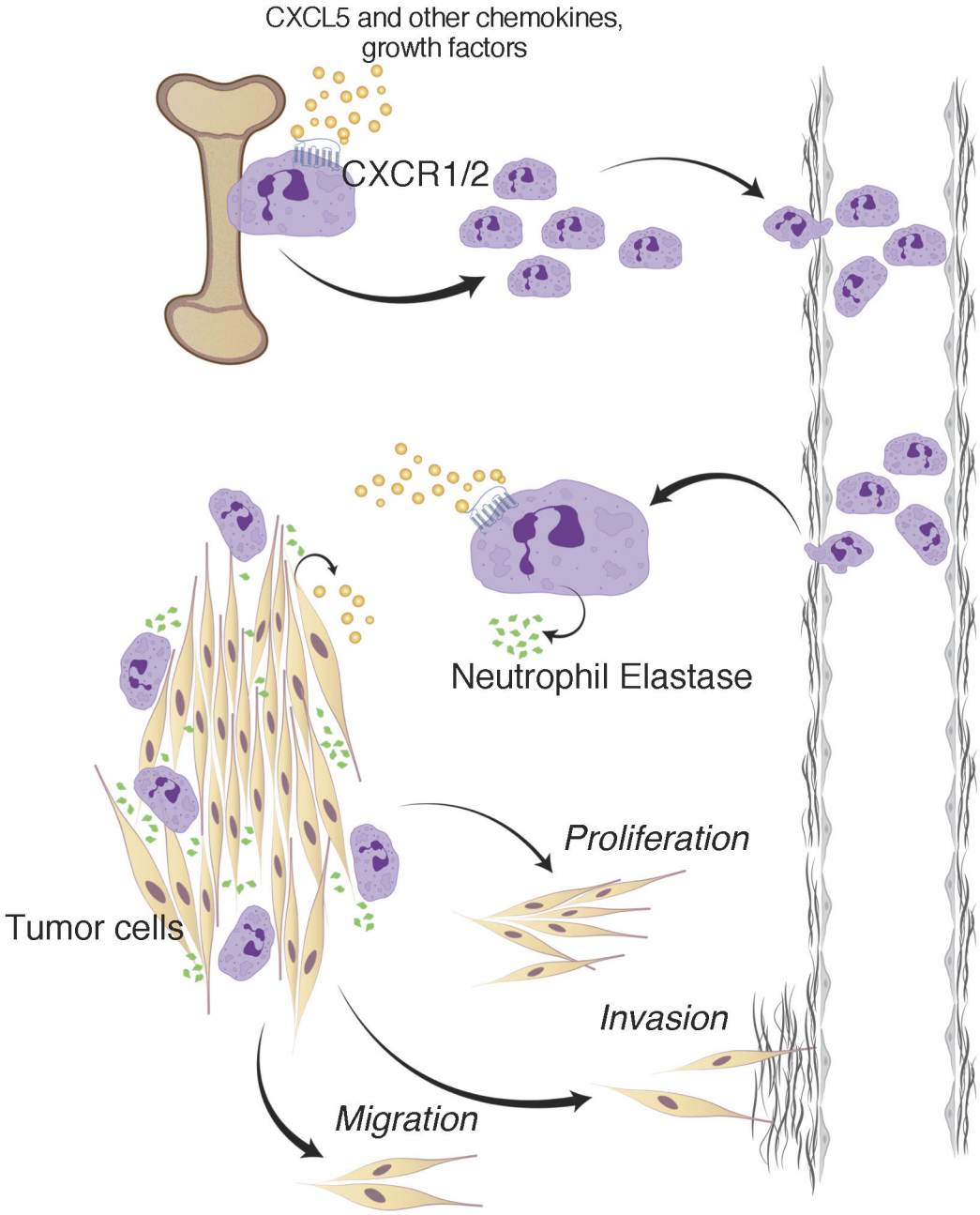

Figure 8. MDSC and NE contribution in cancer biology involves regulation of tumor cell proliferation, migration, and invasion.

Bone marrow-derived MDSCs migrate to premetastatic sites where a vicious cycle of chronic inflammation and tumor growth begins. Established tumors produce various tumor-derived growth factors such as CXCL5 that interact with the common MDSC receptors like CXCR1 and CXCR2, leading to MDSC recruitment to tumor sites and possibly recruitment from bone marrow. We hypothesize that stromal PMN-MDSCs (granulocytic) then secrete factors such as NE to promote tumor cell growth, migration, and invasion. Immunodepleting MDSCs (in order to completely eliminate the potential source of NE), abrogation of MDSC recruitment to tumor sites, or pharmacological inhibition of NE activity were all effective in

diminishing intra-tumoral or peripheral populations of MDSCs, obstructing the MDSC migration process, and attenuating tumor growth.